Third-Harmonic Generation and Self-Channeling in Air Using High-Power Femtosecond Laser Pulses

N. Aközbek,[1,2] A. Iwasaki,[3] A. Becker,[4,5] M. Scalora,[2] S. L. Chin,[3] and C. M. Bowden[2]

[1]*Time Domain Corporation, 7057 Old Madison Pike, Huntsville, Alabama 35806*
[2]*U.S. Army Aviation and Missile Command, AMSAM-WS-RD-ST, Huntsville, Alabama 35898-5000*
[3]*Département de Physique, de Génie Physique et d'Optique and Centre d'Optique, Photonique et Laser, Université Laval, Québec, Québec G1K 7P4, Canada*
[4]*Fakultät für Physik, Universität Bielefeld, Postfach 100 131, D-33501 Bielefeld, Germany*
[5]*Max-Planck-Institut für Physik komplexer Systeme, Nöthnitzer Strasse 38, D-01187 Dresden, Germany*

It is shown, both theoretically and experimentally, that during laser pulse filamentation in air an intense ultrashort third-harmonic pulse is generated forming a two-colored filament. The third-harmonic pulse maintains both its peak intensity and energy over distances much longer than the characteristic coherence length. We argue that this is due to a nonlinear phase-locking mechanism between the two pulses in the filament and is independent of the initial material wave-vector mismatch. A rich spatiotemporal propagation dynamics of the third-harmonic pulse is predicted. Potential applications of this phenomenon to other parametric processes are discussed.

Higher harmonic generation is a fundamental process for laser frequency conversion and has found wide applications in the extension of coherent light generation to shorter wavelengths (for recent reviews, see [1]). One of the main challenges in harmonic generation is the limited nonlinear interaction length over which a certain phase relation between the fundamental and harmonic pulses can be maintained in a bulk medium, such as a gas. In recent years, there has been considerable interest in high harmonic generation using intense femtosecond laser pulses focused into various high pressure gases [2–8]: a conversion efficiency as high as 0.1% was reported for third-harmonic (TH) generation in air [2].

It has been demonstrated both in the near IR [9–13], and the UV [14,15], that long self-induced filaments are generated when subpicosecond high peak power laser pulses are propagated in air. The filaments are created by a dynamic interplay between several mechanisms. First, the spatial intensity profile of the laser pulse acts like a focusing lens due to the optical Kerr effect, which causes the beam to self-focus resulting in an increase of the peak intensity. Second, this process is balanced and stabilized by various nonlinear effects, e.g., the defocusing of the pulse from a low-density electron plasma, and higher-order terms of the nonlinear index of refraction [16]. The dynamics of the filamentation is complex and different interpretations as the moving focus picture [11], the self-channeling model [9,10,12], or spatial replenishment [17] have been proposed. The peak intensity in these long filaments is found to be clamped down to about 5×10^{13} W/cm² [5,18] which is sufficient to generate higher harmonics [2–8].

In this Letter, we report a novel two-colored filamentation effect with the generation of an intense, ultrashort TH pulse that maintains both its peak intensity and energy over the entire length of the filaments, a distance that is many coherence lengths. We will show below that this is due to a nonlinear phase-locking mechanism between the fundamental and TH pulses.

A rigorous theoretical analysis of the propagation of an intense ultrashort laser pulse in gases at high pressure requires the inclusion of the full spatiotemporal dynamics of both the fundamental and the TH pulses. Our model is described by a set of coupled equations, which can be written in dimensionless form in the retarded coordinate system ($\tau = t - z/v_g(\omega)$) as:

$$\left(i\frac{\partial}{\partial z} + \frac{1}{4}\nabla_\perp^2 - i\frac{L_{DF}}{4L_d}\frac{\partial^2}{\partial \tau^2} + i\frac{L_{DF}}{L_{Abs}}|\mathcal{E}_\omega|^{2n-2} \right)\mathcal{E}_\omega +$$
$$\frac{L_{DF}}{L_{NL}}(|\mathcal{E}_\omega|^2\mathcal{E}_\omega + \mathcal{E}_\omega^{*2}\mathcal{E}_{3\omega} + 2|\mathcal{E}_{3\omega}|^2\mathcal{E}_\omega) - \frac{L_{DF}}{L_{PL}}N_e\mathcal{E}_\omega = 0,$$

(1)

$$\left(i\frac{\partial}{\partial z} + \frac{1}{12}\nabla_\perp^2 + i\frac{L_{DF}}{L_{\Delta v}}\frac{\partial}{\partial \tau} - i\frac{L_{DF}}{4L_d'}\frac{\partial^2}{\partial \tau^2} + \frac{L_{DF}}{L_{\Delta k}} \right)\mathcal{E}_{3\omega} -$$
$$\frac{L_{DF}}{3L_{PL}}N_e\mathcal{E}_{3\omega} + i\frac{L_{DF}}{L_{Abs}}|\mathcal{E}_{3\omega}|^{2n-2}\mathcal{E}_{3\omega} +$$
$$\frac{3L_{DF}}{L_{NL}}\left(|\mathcal{E}_{3\omega}|^2\mathcal{E}_{3\omega} + \frac{\mathcal{E}_\omega^3}{3} + 2|\mathcal{E}_\omega|^2\mathcal{E}_{3\omega} \right) = 0,$$

(2)

$$\frac{\partial N_e(\tau)}{\partial \tau} = (\Gamma_\omega + \Gamma_{3\omega})[1 - N_e(\tau)].$$

(3)

Here, $\mathcal{E}_\omega$ and $\mathcal{E}_{3\omega}$ are the electric field envelope functions, normalized to the peak value of the input pump field $\mathcal{E}_0 = \sqrt{2P_0/\pi w_0^2}$; the transformation $\mathcal{E}_{3\omega} \rightarrow \mathcal{E}_{3\omega}e^{i\Delta kz}$ was also used. The subscripts and superscripts, ω and 3ω, denote the fundamental and TH pulses, respectively. The propagation direction z is given in units of $L_{DF} = k_\omega w_0^2/2$, the

temporal coordinate τ in units of the input pulse width τ_0, and the transverse coordinate r in units of the input beam radius w_0. The following length scales are also used: $L_{NL} = (n_2 k_\omega I_0)^{-1}$ is a nonlinear length scale, where $I_0 = |\mathcal{E}_0|^2$, $n_2 = 4 \times 10^{-19}$ cm^2/W, and $L_{PL} = k_\omega m_e c^2 / 2\pi e^2 N_0$ is the plasma length scale, where N_0 is the number density of neutral air molecules. $L_{\Delta v} = [v_g^{-1}(3\omega) - v_g^{-1}(\omega)]^{-1}\tau_0$, represents the characteristic temporal walkoff distance due to the group-velocity mismatch between the two pulses. $L_d = \tau_0^2/2k_\omega''$ and $L_d' = \tau_0^2/2k_{3\omega}''$ are the length scales due to group-velocity dispersion of the fundamental and third harmonic, respectively, where $k_\omega'' = 0.2$ fs^2/cm and $k_{3\omega}'' = 1.0$ fs^2/cm. Finally, $L_{\Delta k} = |\Delta k|^{-1} = |3k_\omega - k_{3\omega}|^{-1}$ is the linear wave vector mismatch length scale in the wave vectors $k_\omega = n_\omega k_0$ and $k_{3\omega} = n_{3\omega} 3k_0$, where $\Delta k = 3k_0(n_\omega - n_{3\omega}) = -5.0$ cm^{-1}. Electron generation through multiphoton ionization of N_2 and O_2 is taken into account by the rates Γ_ω and $\Gamma_{3\omega}$, which are approximated by fitting the ionization rates into the form σI^n for the relevant intensity range, using the *model* of Muth-Böhm *et al.* [19]. The electron density N_e is normalized to N_0, and $L_{Abs} = N_0 \sigma / 2n\hbar\omega$ accounts for ionization losses.

For the numerical simulations we have considered the propagation of a linearly polarized, collimated Gaussian input laser pulse with a center wavelength at $\lambda_0 = 800$ nm, a beam radius $w_0 = 0.49$ cm, and a pulse duration $\tau_{FWHM} = 45$ fs; this is then focused with a lens of focal length of $f = 100$ cm in air at atmospheric pressure. We have used laser input powers, P_0, below and above the critical power, $P_{cr} = \lambda_0^2/2\pi n_\omega n_2 = 3$ GW needed for self-focusing and filamentation. The set of equations, Eqs. (1)–(3), is integrated numerically with the initial condition $\mathcal{E}_{3\omega}(z = 0) = 0$.

The results for the on-axis peak intensity of the pump [Fig. 1(a)] and the TH pulses [Fig. 1(b)] are shown as functions of the propagation distance. As can be seen from Fig. 1(a), in the linear focusing limit ($P_0 = 0.1P_{cr}$, solid line), no distortion of the pump pulse occurs, and the pulse comes to a focus at the geometrical focus. As the input power is increased to $P_0 = 1.5P_{cr}$ (dotted line) and $P_0 = 3.0P_{cr}$ (dashed line), the pump pulse self-focuses before the geometrical focus, and its peak intensity remains nearly unchanged over a distance of several centimeters; i.e., the pump pulse undergoes filamentation. From Fig. 1(b) we see that above the critical power also a filamentation of the third harmonic occurs.

The cofilamentation becomes also obvious from the TH conversion efficiency, shown in Fig. 1(c). For input powers above P_{cr}, the conversion efficiency does not increase further with increasing input power: this is expected since the pump intensity is clamped but the length of the filament increases. The TH energy is roughly constant over the length of the filament, which is a distance much longer than the characteristic coherence length, $L_c = \pi/|\Delta k| = 0.63$ cm, ($P_0 = 1.5P_{cr}$ dotted line, $3.0P_{cr}$

dashed line). In addition, for the current parameters $L_{\Delta v} = 20$ cm; consequently, there is no apparent temporal walk-off between the fundamental and TH pulses. This means that the TH pulse travels inside the filament with nearly the same group velocity as the fundamental pulse. Furthermore, the TH pulse does not give back its energy to the pump pulse, even well after the filament has ceased. On the contrary, for $P_0 = 0.1P_{cr}$ (solid line) the efficiency reaches a maximum at the geometrical focus, but drops rapidly on both sides of the focus. This is due to
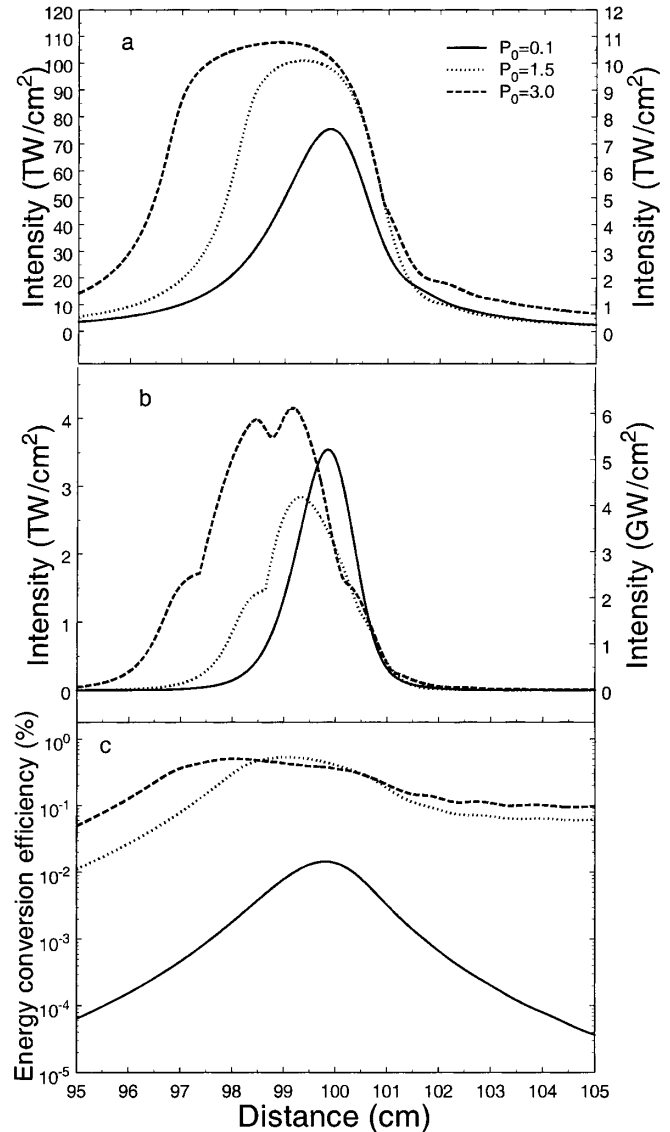

FIG. 1. Numerical results for the on-axis peak intensity of (a) the fundamental pulse and (b) the TH pulse for $P_0 = 0.1P_{cr}$ (solid line) [right-hand scale], $P_0 = 1.5P_{cr}$ (dotted line) and $P_0 = 3.0P_{cr}$ (dashed line) [left-hand scale] as a function of the propagation distance. In (c) the total conversion efficiency as a function of propagation distance is shown. The beam was focused with a lens of $f = 100$ cm.

the typical π-phase shift of the fundamental pulse as it crosses the geometrical focal plane.

To test the results of the calculations, we have performed an experiment using a 1 kHz Ti:sapphire laser chain, which produces pulses with a central wavelength at 800 nm, a pulse duration of 45 fs (FWHM), and a beam radius ($1/e^2$) of ($0.49 \pm 2\%$) cm. Pulses with energy of ($468 \pm 5\%$) μJ were focused into air using a 100 cm focal length lens. A filament about 10 cm in length and a diameter of about 100 μm was observed. In order to measure the TH pulse energy at various positions in the filament, we displaced a diamond pinhole (400 μm in diameter) along the filament [11]. At the position of the pinhole, both the pump and the generated TH pulses pass through, while the filament is terminated beyond the pinhole. The pulses were separated by two successive gratings and the energy of the fundamental and third harmonic were measured by a photodiode and photomultiplier, respectively.

In Fig. 2 the experimental data for the pump and the TH pulse energies (defined as the values contained within the 400 μm diameter) along the filament length are shown. The data confirm the predictions of the calculations, that the pump pulse energy (circles, left-hand scale) *and* the TH pulse energy (triangles, right-hand scale) remain constant over the whole length of the filament. We note that the maximum experimental conversion efficiency of about 0.2% agrees well with the numerical calculations as well as previous observations [2,4,8]. Further, the start of the filament occurs at the same position (about 96 cm) in the experiment and the numerical calculations; however, its length is slightly longer in the experiment.

The results of the numerical calculations and the experiments show that both pulses propagate together without any apparent dephasing effects. In order to provide an explanation, we reexamine Eqs. (1) and (2) in terms of the amplitudes and slowly varying phases using $\mathcal{E}_{\omega,3\omega} = A_{\omega,3\omega} \exp(i\phi_{\omega,3\omega})$ and separate the real and imaginary parts to obtain (for the sake of simplicity, group-velocity dispersion and absorption losses are neglected):

$$\frac{1}{2}\frac{\partial A_\omega^2}{\partial z} = -\frac{1}{4}\nabla_\perp(A_\omega^2 \nabla_\perp \phi_\omega)$$
$$+ \frac{L_{DF}}{L_{NL}}A_\omega^3 A_{3\omega}\sin(3\phi_\omega - \phi_{3\omega}), \qquad (4)$$

$$\frac{\partial \phi_\omega}{\partial z} = -\frac{1}{4}(\nabla_\perp \phi_\omega)^2 + \frac{1}{4}\frac{\nabla_\perp^2 A_\omega}{A_\omega} - \frac{L_{DF}}{L_{PL}}N_e$$
$$+ \frac{L_{DF}}{L_{NL}}[A_\omega^2 + 2A_{3\omega}^2 + A_\omega A_{3\omega}\cos(3\phi_\omega - \phi_{3\omega})].$$

$$(5)$$

In the absence of TH generation (i.e., $A_{3\omega} = 0$), the assumptions of a flat wave front, $\nabla_\perp \phi_\omega \approx 0$, and of a balance between self-focusing and defocusing gives $\frac{\partial A_\omega^2}{\partial z} \approx 0$ and $\frac{\partial \phi_\omega}{\partial z} \approx 0$. This provides the basis for laser
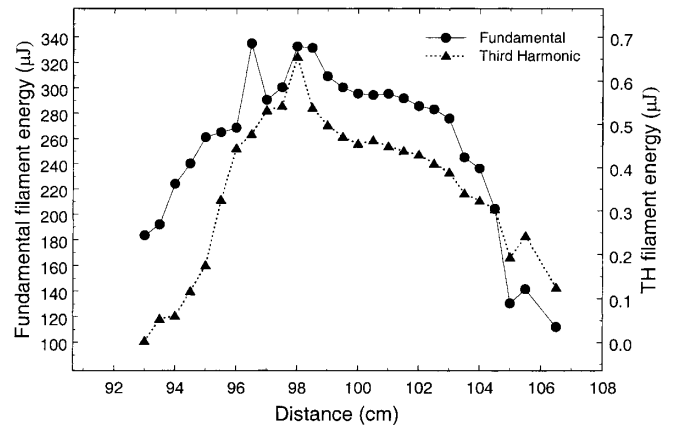

FIG. 2. Experimentally observed pump pulse (circles, [left-hand scale]) and TH pulse (triangles, [right-hand scale]) filament energy, defined as the total energy contained in a 400 μm diameter, as a function of the propagation distance.

pulse filamentation with a constant pulse amplitude [20]. In order to maintain $\frac{\partial A_\omega^2}{\partial z} \approx 0$ (intensity clamping) in the presence of TH generation, the condition $\sin(3\phi_\omega - \phi_{3\omega}) \ll \gamma = (\frac{L_{DF}}{L_{NL}}A_\omega^3 A_{3\omega})^{-1}$ must also be fulfilled [cf. Eq. (4)]. In the present calculations $\gamma \approx 10^{-7}$ for $P_0 > P_{cr}$, which implies that the phase difference $\Delta\phi = 3\phi_\omega - \phi_{3\omega} \approx 0, \pi$ between the two pulses is maintained.

During the self-focusing process, the wave front of the TH pulse follows that of the pump in amplitude and slowly varying phase [due to the source term $\mathcal{E}_\omega^3$ in Eq. (2)], and consequently at the self-focus both wave fronts are flat and $\nabla_\perp \phi_{3\omega} \approx 0$. By analyzing amplitude and phase of the third harmonic in Eq. (2) and following the steps above, we find that $\frac{\partial A_{3\omega}^2}{\partial z} \approx 0$ and $\frac{\partial \phi_{3\omega}}{\partial z} \approx 0$, when $\cos(3\phi_\omega - \phi_{3\omega}) \approx -1$, in agreement with the previous condition $\sin(3\phi_\omega - \phi_{3\omega}) \approx 0$. Thus, filamentation of the generated TH pulse occurs intrinsically together with the filamentation of the pump pulse, independent of the material wave-vector mismatch. Inside the filament, the two pulses are coupled together in a quasi-steady-state condition with constant envelope phase difference, thus forming a two-colored filament.

Because of the close correlation between the fundamental and TH pulses, it is expected that the TH pulse will exhibit a rich spatiotemporal dynamics as predicted for the fundamental pulse [16,17]. In Fig. 3 we show the contour intensity distribution of the fundamental (left column) and TH (right column) pulses for $P_0 = 3.0P_{cr}$ at (a) $z = 97$ cm, (b) $z = 98$ cm, and (c) $z = 101$ cm. At the beginning of the filament [Fig. 3(a)], the fundamental and the TH pulses have been self-focused to a beam diameter of about 100 microns, which is in good agreement with our experimental observations. At a further propagation distance Fig. 3(b), the back of the pulse is defocused by the plasma generated by the front of the pulse, which corresponds to blueshifting [16], in
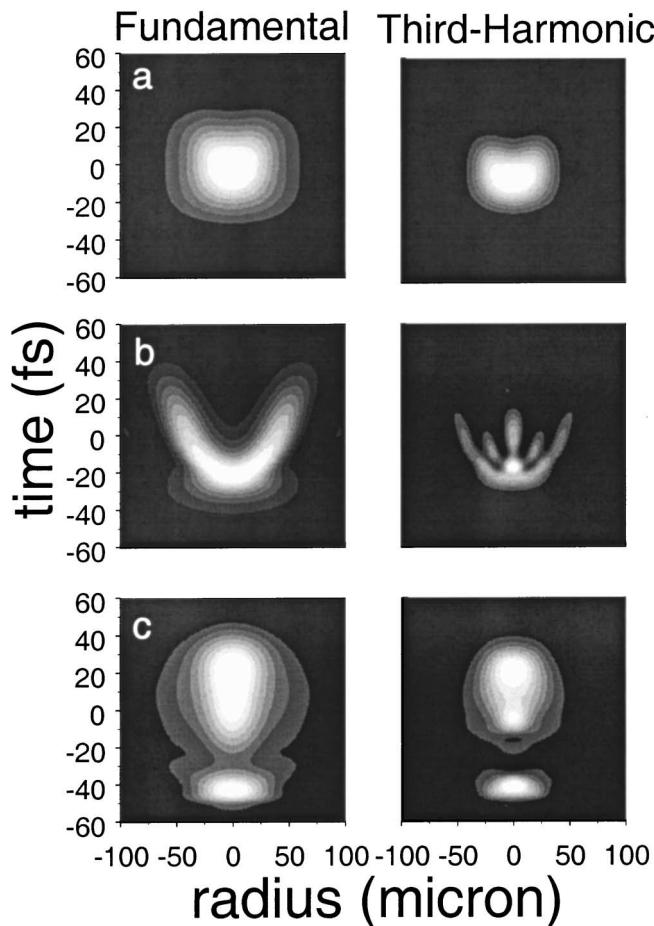
FIG. 3. Numerical results for the spatiotemporal intensity distribution of the fundamental pulse (left) and TH pulse (right) at (a) $z = 97$ cm, (b) $z = 98$ cm, and (c) $z = 101$ cm. The input power is $P_0 = 3.0 P_{cr}$.

agreement with previous experimental observations [2,3]. Finally, the back of the pulse refocuses with the appearance of temporal pulse splitting of both the fundamental and TH pulses [Fig. 3(c)].

This natural scheme of nonlinear conversion over distances much longer than the usual coherence length is expected to appear during the filamentation in other gases and condensed media as well. We also expect that other types of third-order parametric processes such as four-wave mixing, parametric amplification and higher-order harmonic generation could be achieved by this phenomenon leading to multicolored filaments.

Finally looking ahead, if even longer two-colored filaments are possible, this kind of phase-locked propagation of TH pulse should be useful for various applications of laser pulse propagation in air. For example, the potential

of the supercontinuum or white-light continuum spectrum, generated by the fundamental IR pulse during the filamentation process, for atmospheric sensing has been demonstrated recently [21]. Efficient TH generation over long distances would extend the spectral region of this novel atmospheric sensing method further in the UV and could potentially enable the simultaneous monitoring of chemical pollutants and biological species.

In conclusion, we have shown that during the propagation of an ultrashort high-power laser pulse in air a TH is generated, which maintains its energy and intensity over distances much longer than the characteristic coherence length. The results of numerical calculations for this phenomenon are confirmed by experimental data. It is argued that this two-color filamentation effect is due to a nonlinear phase-locking mechanism which couples the fundamental and the TH pulse together, with constant phase difference inside the filament.

[1] P. Salieres, A. L'Huillier, and M. Lewenstein, Adv. At. Mol. Opt. Phys. **41**, 83 (1999); T. Brabec and F. Krausz, Rev. Mod. Phys. **72**, 545 (2000).
[2] S. Bachus et al., Opt. Lett. **21**, 665 (1996).
[3] C. W. Siders et al., J. Opt. Soc. Am. B **13**, 330 (1996).
[4] A. B. Fedotov et al., Opt. Commun. **133**, 587 (1997).
[5] H. R. Lange et al., Phys. Rev. Lett. **81**, 1611 (1998).
[6] Y. Tamaki et al., Phys. Rev. Lett. **82**, 1422 (1999).
[7] G. Marcus, A. Zigler, and Z. Henis, J. Opt. Soc. Am. B **16**, 792 (1999).
[8] Zhu Chang-jun et al., Chin. Phys. Lett. **18**, 57 (2001).
[9] A. Braun et al., Opt. Lett. **20**, 73 (1995).
[10] E. T. J. Nibbering et al., Opt. Lett. **21**, 62 (1996).
[11] A. Brodeur et al., Opt. Lett. **22**, 304 (1997).
[12] H. R. Lange et al., Opt. Lett. **23**, 120 (1998).
[13] L. Wöste et al., Laser Optoelektron. **29**, 51 (1997).
[14] J. Schwarz et al., Opt. Commun. **180**, 383 (2000).
[15] S. Tzortzakis et al., Opt. Lett. **25**, 1270 (2000).
[16] N. Aközbek, C. M. Bowden, and S. L. Chin, Opt. Commun. **191**, 353 (2001).
[17] M. Mlejnek, E. M. Wright, and J. V. Moloney, Opt. Lett. **23**, 382 (1998).
[18] A. Becker et al., Appl. Phys. B **73**, 287 (2001).
[19] J. Muth-Böhm, A. Becker, and F. H. M. Faisal, Phys. Rev. Lett. **85**, 2280 (2000).
[20] Y.-R. Shen, *Principles of Nonlinear Optics* (Wiley, New York, 1984).
[21] P. Rairoux et al., Appl. Phys. B **71**, 573 (2000).